INTERNATIONAL ATOMIC ENERGY AGENCY
UNITED NATIONS EDUCATIONAL, SCIENTIFIC AND CULTURAL ORGANIZATION

INTERNATIONAL CENTRE FOR THEORETICAL PHYSICS
34100 TRIESTE (ITALY) - P.O.B. 586 - MIRAMARE - STRADA COSTIERA 11 - TELEPHONE: 9240-1
CABLE: CENTRATOM - TELEX 460392-I

H4.SMR/222 - 15

SECOND AUTUMN WORKSHOP ON
CLOUD PHYSICS AND CLIMATE

(23 November - 18 December 1987)

IMPACT OF PHYSICAL PROCESSES ON SIMULATION AND MEDIUM-RANGE PREDICTION OF THE ASIAN SUMMER MONSOON

U.C. MOHANTY
IIT, Delhi
India

TOPIC VI-4

IMPACT OF PHYSICAL PROCESSES ON SIMULATION AND MEDIUM-RANGE PREDICTION OF THE ASIAN SUMMER MONSOON

U. C. Mohanty

Centre for Atmospheric Sciences
India Institute of Technology
Haus Khas, New Delhi, 110016 India

1. INTRODUCTION

It has been recognised that the onset of the Asian summer monsoon is that part of the seasonal transition of the general circulation from a winter to a summer regime over Asia. The most conspicuous features of the transition are (1) the outburst of a low-level (850 mb) westerly jet off the east coast of Africa and the Arabian Sea, called the Somali Jet; the establishment of an upper tropospheric (150 mb) easterly jet over the Indian peninsula and the adjoining seas, known as the Tropical Easterly Jet (TEJ), (3) and the intensification of a large sub-tropical anticyclone over the Himalayas at about 150 mb and (4) a shift of the westerly jet to the north of the Himalayas. The numerical simulation results from FGGE data by a number of investigators (Krishnamurti and Ramanathan, 1982); Mohanty, et al., 1984, etc.) indicate that the intensification of the monsoon flow is mainly dictated by release of convective instability and is very sensitive to the intensity and location of diabatic heating in the troposphere (i.e., diabatic forcing in the model). Consequently, the simulation of tropical convection, including its intimate links with surface processes (vertical fluxes of heat and moisture) and radiation is one of the main problems for simulation and prediction of the monsoon. The main effect of all of these physical processes is the intensification of the tropical diabatic heat source through an intensified hydrological cycle by enhanced moisture supply and increased precipitation in the tropics. Thus, the summer monsoon onset over the Indian subcontinent, which is marked by rapid intensification of both jets over a period of few days and a major transition in the global atmospheric circulation, is probably the best case for the sensitivity experiments to illustrate the impact of physical processes on the performance of numerical models over the tropics.

Observations from diverse observing systems from the First GARP Experiment (FGGE), including that from the summer monsoon experiment (MONEX) have provided an excellent data base for numerical experiments; in particular, this data have provided the best analysis yet produced of an onset event, that of 1979, and this event is the obvious choice for the present study.

This paper describes the results of a series of 10-day forecasts to assess the model's simulation of the onset of the summer monsoon. In each forecast some aspects of the physical processes was altered/dropped and its impact on the model's performance assessed. Each integration started from 12 June 1979 and covered the rapid intensification of the Asian summer monsoon, which took place in the subsequent days. Following the description of the model, initial conditions, various parameterization schemes and numerical experiments in Section 2, the results are presented and discussed in Section 3. The main conclusions are summarized in Section 4.

2. DESCRIPTION OF THE EXPERIMENTS

2.1 Model description

The integrations were performed with the ECMWF T-63 spectral model (Simmons and Jarradu, 1984). The model has 16 levels in the vertical based on a hybrid co-ordinate system (Figure 1). The model includes a comprehensive set of physical processes based on those described by Tiedtke, et al., (1979).

2.2 Description of modified parameterization scheme

Modified Kuo scheme

Four modifications have been made to the original Kuo-scheme (Anthes, 1977); Tiedtke, et al, 1979) in the model.

(a) Cloud base: is defined as the condensation level for surface air and can occur within a well mixed boundary layer (this was previously linked to the height of the well mixed boundary layer). This change enhances the occurrence of cumulus convection and gives a more realistic response, by the convection, to the diurnal cycle in surface heating of the tropical land masses;

(b) Cloud ascent is determined considering only condensation (no ice pahse);

(c) The moistening parameter β.

$$\beta = 1 - \frac{\int_{P_{top}}^{P_{base}} RH \, dp}{P_{base} - P_{top}} = 1 - \bar{U}$$

where P top and P base are the pressure of the top and base of the cloud, U is the average relative humidity in the cloud layer in its original form tends to over moisten the environment and to underestimate the latent heat release. In the modified code the moistening parameter is replaced by β^3, which with its stronger dependency on the environmental saturation deficit, gives less moistening and more heating and thus reduces the model's tendency to generate states which are too cold and too moist;

(d) Multi-layered cumulus convection is no longer considered for simplification of the code.

The net effect of all these changes is to give a much improved structure in convective situations.

Shallow convection

A parameterization scheme for shallow convection, not previously incorporated, has been developed in which the turbulent transports of sensible heat and moisture are represented by vertical diffusion within moist convectively unstable layers, through cloud base and through the levels of non-

buoyancy. The parameterization of the mean temperature and moisture changes due to shallow convection (condensation not considered) take the form of:

$$\left(\frac{\partial \bar{T}}{\partial t}\right)_{CU} = \frac{1}{\bar{\rho} c_p}\frac{\partial M}{\partial z}$$

$$\left(\frac{\partial \bar{q}}{\partial t}\right)_{CU} = \frac{1}{\bar{\rho}}\frac{\partial N}{\partial z}$$

where $M = C_p \bar{\rho}\left(\frac{p}{p_0}\right)^{R/C_p} K \frac{\partial \bar{T}}{\partial z}$; $N = \bar{\rho} K \frac{\partial \bar{q}}{\partial z}$

The eddy diffusivity K is taken as constant at 25 $m^2 S^{-1}$ in the cloud layer (not above 750 mb) and zero elsewhere. A full description of the scheme and a preliminary assessment is given in Tiedtke (1985). The scheme effectively transports moisture form the boundary layer into a cloud layer above. This is most pronounced in the trades, where shallow convection counteracts the drying and warming effect of the mean subsidence. The shallow cloud layer extends over several model layers and the depth of the total moist layer is considerably deeper.

Revised infrared radiation scheme

The original ECMWF radiation scheme was based on a two-stream approximation of the radiative transfer equation both in the solar and infrared part of the spectrum (Geleyn and Hollingsworth, 1979). In both wave domains an effective absorber path length method (EAM) was used to incorporate the effects of gaseous absorption and emission. This method works well in the shortwave but the approximations that are necessary in the longwave to make the scheme computationally viable have led to problems, in particular with the treatment of the emission terms in the atmosphere. The scheme gives excessive cooling rates in layers with small amounts of scaterer due to clouds and aerosols (Slingo, 1982). To overcome this problem a longwave radiation scheme with a revised treatment of gaseous absorption has been developed. This is based on the technique of exponential sum fitting (ESFT) in which the gaseous transmission function is approximated by a series of decaying exponentials. Each exponent behaves like a monochromatic optical depth which can be easily incorporated into the multiple scattering form of the existing radiation scheme. A computationally efficient version of this method (FESFT) which simplifies the treatment of gaseous overlap has been developed (Ritter, 1984). This scheme gives a much more realistic response to small amounts of cloud. The EAM scheme exhibits a strong cooling near 600 mb even though the corresponding cloud cover is small. It also underestimates the cooling near the surface associated with the rapid increase in humidity.

2.3 Initial conditions and experiments

All integrations start from real data from the FGGE observing period. A starting date of 12Z, 11 June 1979, was chosen so as to cover the period of rapid intensification of the monsconal flow over India. For these experiments the FGGE level-IIb data is re-analysed using the present operation analysis procedure of the ECMWF. Data assimilation was started from 5 June 1979 using the revised system described by Lonnberg and Shaw (1983). A non-linear diabatic normal mode initialization with only the first five vertical modes (Werger, 1983) is carried out for initialization of the input data.

The results from five experiments are described - one control and four integrations in which some aspects of physics was modified/dropped. Table 1 gives a list of the experiments and indicates which part of the physics was modified/dropped. If no change is indicated then the control run counterpart is used.

TABLE 1

Numerical experiments with modification to the physical processes

Experiment	Modified Kuo plus shallow convection	New Radiation	Remarks
W81	-	-	Control: ECMWF operational model as on 1 December 1984
X20	X	-	To study the impact of convection
X31	-	X	To study the impact of only radiation
Y68	X	X	To examine the response of convection and radiation
BON	X	No Radiation	To illustrate the influence of radiation on convection

3. RESULTS

3.1 Impact of the physical processes on tropical forecast

The tropical flow is, as expected, most influenced by the physical processes in the model. Improvement of parameterization schemes and inclusion of shallow convection in the model reduces the systematic errors in large-scale diabatic heating, and the large-scale flow. This may be attributed to an overall increase of the hydrological cycle (moisture supply and precipitation rate), and diabatic heating as a consequence. In this section a legend discussion on the impact of the physical processes on simulation and medium-range prediction over the entire tropical belt will be presented.

Figure 2 illustrates the time evolution of the root mean square (RMS) vector wind errors at 850 mb for the tropical strip (35°S-32°N). The graphs include persistence, so that the skill of the forecast can be assessed. As may be seen, the control experiment (W81) develops substantial errors by the end of the forecast, both in the total field and for the very long waves (1-3) where it is worse than persistence for most of the forecast. The introduction of an improved longwave radiation scheme (X31) gives an improvement in total errors, but a lesser change for the very long waves (Figure 2a), particularly torwards the end of the forecast. In comparison, the introduction of shallow

convection and a modified Kuo scheme (X20) gives only a small improvement in total errors, but a dramatic effect on the large-scale flow (Figure 2b). It is interesting to note that the full benefits of convection changes are only realised when they are combined with the radiation changes. Then the errors decrease still further, so that the forecast is better than persistence throughout (Figure 2b). The best results are obtained only when all the changes to the physics are incorporated. Figure 2 shows that the model responds quite rapidly to improvements in the physics. By day 4 the effect of shallow convection and modified Kuo (X20 vs. W81) is already established (Figure 2b). The radiation changes are also evident by day 4 but a further response can also be seen later in the forecast (X31 vs. W81; X20 vs. Y68).

To see what these root mean square errors mean in terms of flow patterns simulated by the model, the observed mean flow patterns at 850 mb for days 5-10 of the forecast (i.e., 16-21 June 1979) together with forecast errors, are illustrated in Figure 3. The control experiment (W81) shows the spurious westerly flow over W. Africa which was a typical feature of the ECMWF operational model. It does not predict the extent of the observed intensification of the Somali jet, and also fails to predict the observed strong low-level easterlies over the tropical Atlantic (Figure 3e). With the introduction of shallow convection and a modified Kuo (X20) scheme the marked improvement in the large scale flow evident in Figure 3d, is seen in the strengthening of trade winds over the Atlantic, and the removal of the spurious westerlies over Africa. The monsoonal flow, however, is still not well simulated. On the other hand, the modified radiation scheme improves the monsoon forecast, but has little effect on the flow over the Atlantic and West Africa. It is only when the convection changes are combined with the radiation changes (Y68) that there is a substantial improvement in prediction over the tropical belt. The same result is evident in the winds at 200 mb (not shown). The best results are again obtained only when shallow convection and changes in convection and radiation are incorporated in the model.

The model precipitation patterns (Figure 4) show marked differences associated with different changes in the physical processes. The control experiment (W81) is characterised by excessive precipitation over Indonesia and a weak ITCZ, when compared with climatological estimates for June from Jaeger (1976). The monsoonal rains over India are also underestimated. The new radiation scheme tends to increase radiative cooling in the lower troposphere near the surface. The new scheme tends to stabilise the lower troposphere, while the old scheme tends to destabilise it quite rapidly. The result of this stabilising tendency is a general reduction in precipitation without affecting its geographical distribution (Figure 4d). The shallow convection and modified Kuo schemes have the greatest impact on precipitation (X20). Compared to the control run (W81) considerably higher precipitation rates occur along the ITCZ downstream of the trades (Atlantic and North Brazil Central Pacific, Indian Ocean) and smaller rates occur over Indonesia (Figure 4b and 4c). The distribution is now much more realistic when compared with Jaeger's climatology (Figure 4a). However, the monsoon rains over India and the Arabian Sea are still underestimated, while the maxima near the Somali Jet and north of the Bay of Bengal seem unrealistically large. It is interesting to note that when the radiation changes are added to convection changes (Y68), there is a marked improvement in these features (Figure 4e), and in the flow pattern (Figures 2 and 3). The monsoon rains are increased over India, while the Arabian Sea and the Bay of Bengal precipitation is reduced.

The large change in precipitation when convection changes are introduced may be attributed primarily to a deeper and more moist trade-wind boundary layer over oceans due to shallow convection. The top of the trade wind cloud layer seems to be higher by about 100 mb, and the higher amount of moisture in trade wind regions is primarily advected into the ITCZ. The moisture balance for the trades implies a larger moisture supply through evaporation from the oceans and this is clearly seen in Figure 5 compared to the control run (W81) the experiment with shallow convection and all changes in convection and radiation (Y68) shows an increase in evaporation rate over large tropical oceanic regions by about 50 Wm^{-2} (equivalent to almost 2 mm day^{-1} of precipitable water), and by about 75-100 mm^{-2} over the equatorial Indian Ocean and the Arabian Sea. The evaporation is now much closer to the climatological value for June (Figure 4a). From Esbensen and Kushnir (1981). The main reason for increased evaporation is the enhancement of the moisture gradient adjacent to the ocean surface due to the vertical transport and mixing in the boundary layer by the shallow convection.

A marked improvement in the flow pattern and hydrological cycle over the entire tropical belt and particularly over the monsoon region occurs only when the improvements in long-wave radiation estimation are combined with the convection changes. It emphasises that a physical process cannot be considered in isolation. Further, the results clearly demonstrate the role of the physical processes in the model for improving tropical forecasts.

3.2 Impact of the physical processes on the simulation of the Asian summer monsoon

The role of physical processes in a realistic simulation of the hydrological cycle (evaporation and precipitation) over the monsoon region has been presented in Section 3.1. In this section the simulation of the monsoon's onset and prediction of the stationary components of the summer monsoon will be illustrated.

Time sequences of the kinetic energy (KE) of the 850 mb flow over the Arabian Sea region (0°-22.5°N, 41.25°-75°E) are depicted in Figure 6. The kinetic energy of the analysed flow shows an increase by about five times between 11 and 17 June. The simulation with all revisions to the physics (Y68) clearly performs better than all other experiments. Although in this case KE increases by about 3-4 times between 11-17 June, it still fails to reproduce the observed increase in kinetic energy. The simulation with the modified radiation (X31) performs, to some extent, better than the control (W81), although the growth in KE does not exceed 2-3 times the initial value on 11 June. As already discussed it can be clearly seen that it is only when convection changes are combined with the radiation changes (Y68 vs. X20) that some intensification of the low level flow is simulated. This is consistent with the increased precipitation over the Arabian Sea (Figure 4) in Y68, and agrees with other studies (e.g., Krishnamurti, et al, 1963; Mohanty, et al, 1984). Assessment of the results show that the increase in the diabatic forcing due to a realistic simulation of the hydrological cycle (Figure 4 and 5) primarily leads to a significant improvement in the simulation of the rapid evolution of the monsoon circulation over the Arabian Sea and India.

To examine the skill in the simulation and prediction of the stationary components of the monsoon circulation on the time scale of the medium-range forecast (10-days), the time averaged (days 1-10) winds at 350 mb and 150 mb are illustrated in Figures 7 and 8. Although shallow convection and

a modified Kuo scheme (X20) improves the low-level tropical flow over West Africa and the Atlantic Ocean they fail to intensify the monsoon circulation. The performance of the new radiation scheme (X31) over the monsoon region is quite encouraging. However, the low level cross-equatorial flow off the east coast of Africa and the Somali Jet over the Arabian Sea are realistically simulated only in experiment Y68 (Figure 7e).

Another important feature of the summer monsoon circulation is an upper tropospheric (≈ 150 mb) easterly jet over the Indian Peninsula and adjoining seas. This easterly jet is associated with a strong cross-equatorial return flow (divergent flow). The time averaged wind fields at 150 mb (Figure 9) show that experiments W81 and X31 simulate a strong equatorial zonal flow which was considered to be a systematic error in the ECMWF operational forecasts. With the introduction of shallow convection and modified Kuo (X20) parameterization, a small improvement in the divergent flow is noticed. But it is only when the convection changes are combined with the new radiation scheme (Y68) that the easterly jet along with strong cross-equatorial return flow is realistically simulated. In association with the improved divergent flow over the Indian Ocean in Y68, the excessive easterly flow over Central Africa and the Atlantic is greatly reduced. Thus, a marked improvement in lower and upper tropospheric flow over the monsoon regime occurs only when the convection changes are combined with the new radiation scheme.

The time mean (days 1-10) sectorial averages (45°-75°E) of zonal wind (u), meridional wind (v) and vertical motion (w) over the Arabian Sea are illustrated in Figures 9-11 respectively. The low level westerlies and upper tropospheric easterlies over the Arabian Sea are well simulated in the experiment Y68 (Figure 9). The control run (W81) fails to simulate the low level westerly jet. The experiments X20 and X31 simulate a very weak jet over the Arabian Sea. The low level southerly component of the motion is reproduced well in all these experiments (W81, X20, X31 and Y68), but the upper level cross-equatorial return flow is only properly simulated in the experiment Y68 (Figure 10). The strong ascending motion over the Arabian Sea near 15°N (Figure 11) is reproduced extremely well only in experiment Y68. The other experiments (W81, X20 and X31) failed to simulate this feature.

The remarkable success in simulation and prediction of the detailed features of the zonally averaged fields over the Arabian Sea, which occur only when the radiation changes are combined with the convection changes is a major result of this study. This result illustrates the impact of physical processes on the simulation and prediction of the monsoon circulation. Moreover it emphasises the need of an effective radiation convection interaction in the numerical model for monsoon prediction.

3.3 Impact of radiation-convection interaction on the prediction of tropical circulation

This aspect is well illustrated in Sections 3.1 and 3.2. In this section an attempt will be made to quantify the impact of radiation on convection in the simulation and prediction of the tropical circulation.

For this purpose, a 10-day real data simulation experiment (BGN) was carried out in the absence of radiation in the model. The purpose was to examine the influence of radiation on convection, but shallow convection and the modified Kuo scheme were incorporated in the model.

In the absence of radiative processes the hydrological cycle (precipitations and evaporation) was reduced substantially over the tropics (Figures 4f, 5f, 13 and 14). The ITCZ had almost disappeared over the major part of the tropical belt and remained weak over the monsoon region. Considerable reduction in zonal distribution of convective precipitation (Figure 13) and surface moisture fluxes (Figure 14) were observed in the experiment without radiation (BGN). Convective precipitation was reduced to one third value of its value over the tropics (Y68 vs. BGN). This is reflected in the temperature tendency due to convection. Over the tropical belt the heating rate of about 3°C per day in Y68 (Figure 12) was reduced to a heating of 1°C per day in experiment BGN. This result demonstrates that convective activity is very sensitive to the radiation. In its absence convective activity is reduced by almost half to one third of its value over the tropics (Y68 vs. BGN).

A weak hydrological cycle leads to a weak diabatic forcing in the tropics, which is reflected in the simulation of the stationary components of the monsoon circulation. The low level Somali Jet has almost disappeared over the Arabian Sea (Figure 7f) and the upper level tropical easterly jet is considerably weakened (Figure 8f).

These results clearly demonstrate the response of convection to radiation and emphasise that a physical process cannot be considered in isolation.

CONCLUSIONS

This study has concentrated on the impact of physical processes on the simulation and medium-range weather prediction over the tropics and, in particular, over the monsoon region. On the basis of a number of interesting results discussed above, the following general conclusions may be drawn:

(a) Introduction of shallow convection and a modification of the Kuo convection scheme, along with long-wave radiation parameterization in the model (Y68) have an integral effect by intensifying the hydrological cycle (evaporation and precipitation). This provieds a more realistic and intensified diabatic forcing in the tropics;

(b) The improvement in diabatic heating over the tropics leads to a significant success in simulation and prediction of tropical flow. In particular, the trade winds are much improved along with the precipitation associated with the ITCZ. The erroneous flow over Africa is also largely connected;

(c) The results have shown that the combined effect of improvements in representation of physical processes leads to a significant improvement in simulation and prediction of monsoon circulation, in particular, the precipitation rate, low and upper level jets are handled extremely well in experiment Y68. A major result of this study is the ability of the only experiment Y68 to predict an upper level (≈ 150 mb) divergent flow over the SE Asia and Indian Ocean. These changes can be attributed, to the introduction of shallow convection and the modifications to the deep cumulus convection (Kuo scheme). It is also interesting to note that improvement in radiation parameterization is necessary for realising the benefits of changes in convection. This is particularly evident for the monsoon; without radiation changes, improvements in convection give no intensification of the monsoon circulation. This is also associated with lack of development of monsoon rains over the Arabian Sea and Southern India.

The impact of radiation is further emphasized by a sensitivity experiment (BCN), which was carried out in absence of the radiation parameterization in the model.

References

Anthes, R.A., 1977 : A cumulus parameterization scheme utilizing a one-dimensional cloud model. Mon. Wea. Rev., 105, 270-286.

Esbensen, S.Z. and Kushnir, Y., 1981 : The heat budget of the global ocean. An atlas based on estimates from surface marine observations. Climate Research Institute, Report No. 29, Oregon State University, Corvallis, Oregon.

Geleyn, J.F. and Hollingsworth, A., 1979 : An economical analytical method for the computation of the interaction between scattering and line absorption of radiation. Contr. to Atmos. Physics, 52, 1-16.

Jaeger, L. 1976 : Monatskarten des Niederschlages fur die ganze Erde. Ber Dtsch. We Zerd., Offenbach/Main, No. 139, Vol. 19, 38 pp.

Krishnamurti, T.N. and Ramanathan, Y., 1982 : Sensitivity of the Monsoon onset to differential heating. J. Atmos. Sci, 39, 1290-1306.

Krishnamurti, T.N., Pasch, R.J. and Kitade, T., 1983 : WGNE forecast comparison experiments. Report No. 6, WCRP, WMO, Geneva, pp 73-104.

Lonnberg, P. and Shaw, D., 1983 : ECMWF data assimilation scientific documentation. ECMWF Meteorological Bulletin M1.5/1. Research Manual 1.

Mohanty, U.C., Pearce, R.P. and Tiedtke, M., 1984 : Numerical experiments on the simulation of the 1979 Asian Summer Monsoon. ECMWF Tech. report No. 44, 46 pp.

Ritter, B., 1984 : The impact of an alternative treatment of infrared radiation on the performance of the ECMWF forecast model. Proc. IAMAP International Radiation Symp., 21-29 August, Italy (in press.

Simmons, A.J. and Jarraud, M., 1984 : The design and performance of the new ECMWF operational model, ECMWF seminar on Numerical Methods for Weather Prediction, Septl, 5-9, 1983, ECMWF, Vol. 2, 113-164.

Slingo, J.M., 1982 : Report on a study of the EC radiation scheme, ECMWF Tech. Memo No. 61, ECMWF.

Tiedtke, M., Geleyn, J.F., Hollingsworth, A. and Louis J.F., 1979 : ECMWF Model : Parameterization of subgrid scale processes. ECMWF Tech. Report No. 10, 46 pp.

Tiedtke, M., 1985 : The sensitivity of the time-mean large-scale flow to cumulus convection in the ECMWF model. ECMWF Workshop on convection in large-scale numerical models, 28 Nov. - 1 Dec. 1983, ECMWF, 297-316.

Wergen, W., 1983 : Initialization, ECMWF Seminar/Workshop on Interpretation of numerical Weather prediction products, 13-24, Sept. 1982, ECMWF, 31-57.

Fig. 2

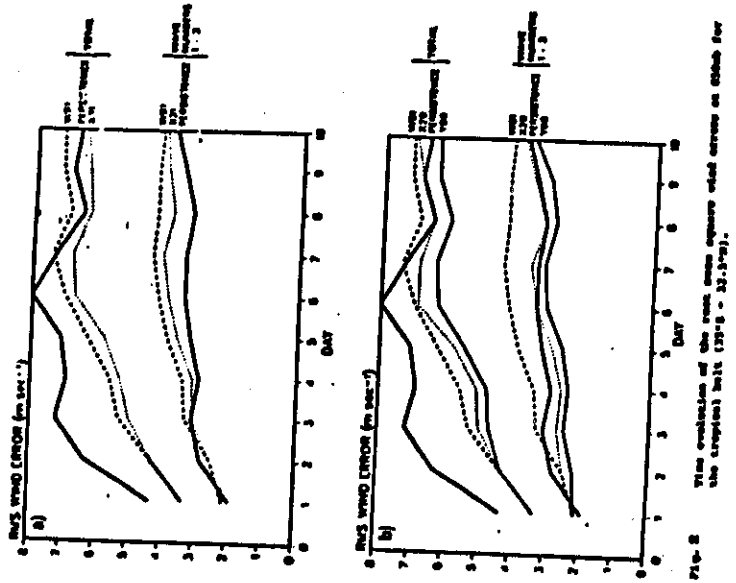

Fig. 1

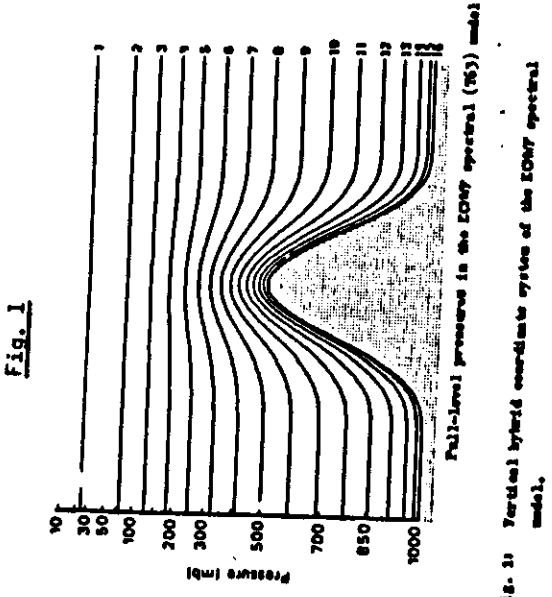

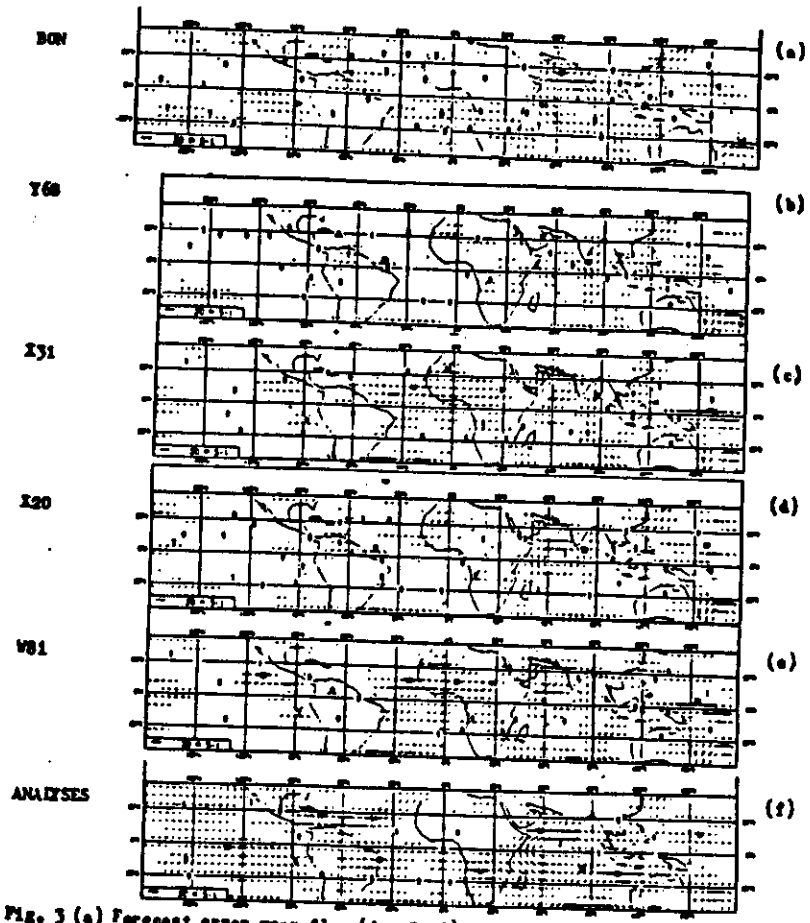

Fig. 3 (a) Forecast error mean flow (day 5-10) vectors at 850 mb, BON; (b) as (a) but for Y68; (c) as (a) but for X 31; (d) as (a) but for X20; (e) as (a) but for W81, (f) mean observed 850 mb wind vector 15-21 June; 1975 (FGGE analysis)

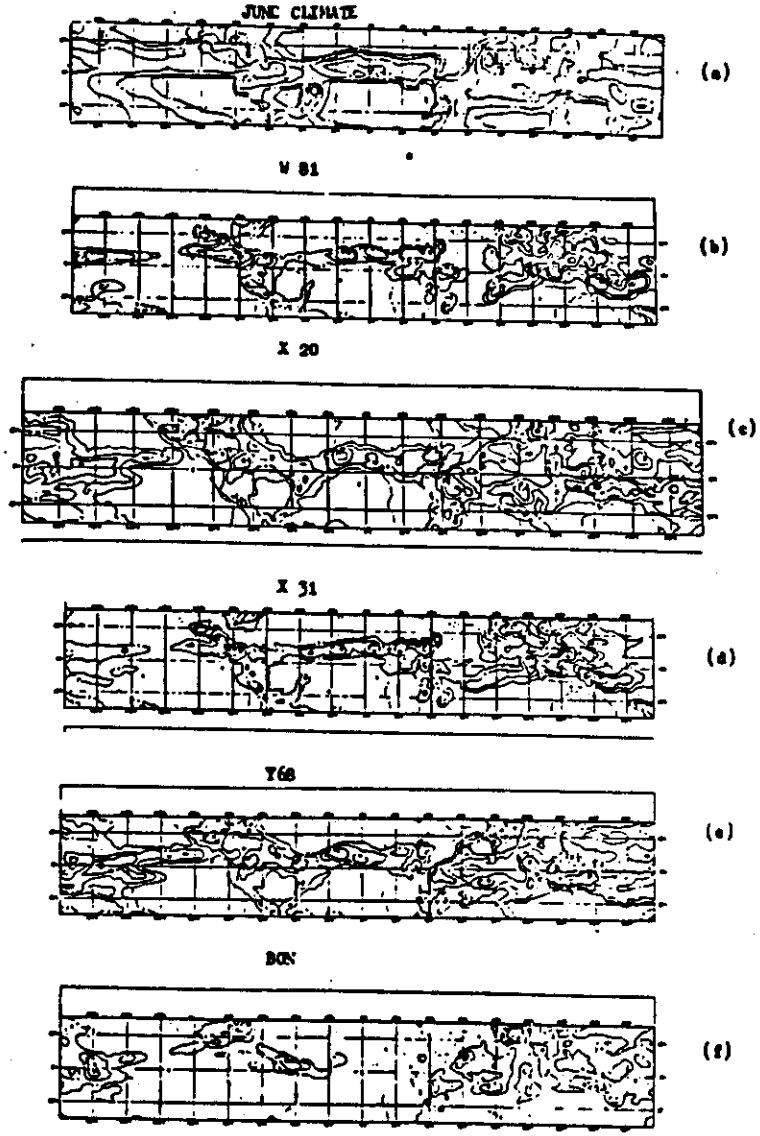

Fig. 4 Ten days mean total precipitation rate (mm day $^{-1}$) (a) Jaeger's climate values for June; (b) W81, (c) X20, (d) X31; (e) Y68, (f) BON.

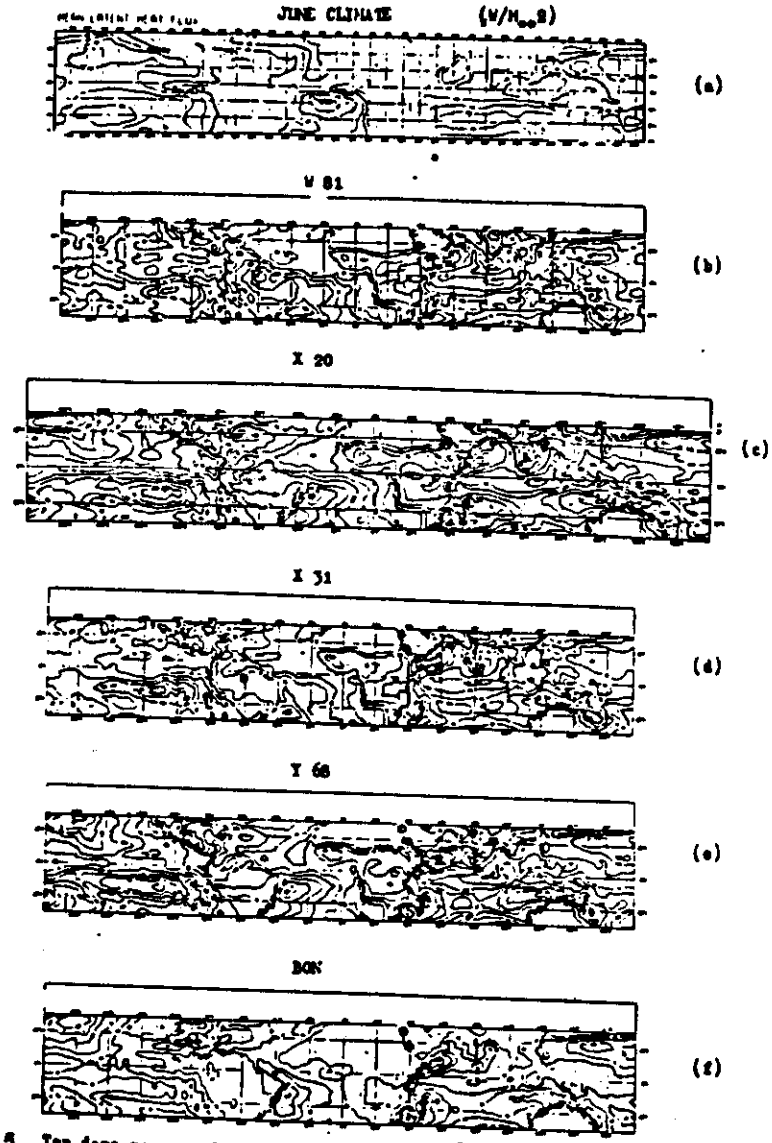

Fig. 5 Ten days mean surface moisture fluxes (Wm^{-2}) (a) climate values over the ocean for June from Esbensen and Kushnir; (b) W81, (c) X20, (d) X31; (e) Y68, (f) DON

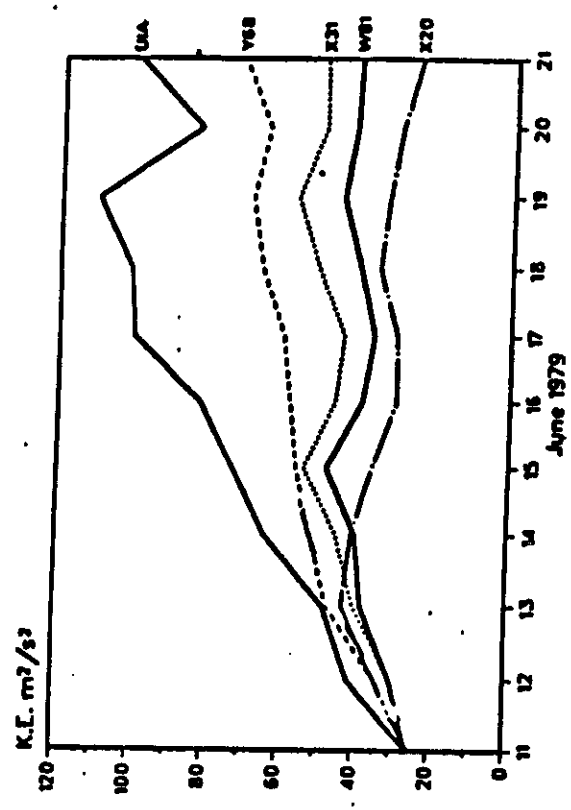

Fig. 6 Time series of the kinetic energy of the 850mb flow over the Arabian Sea region (0-22.5°N, 41.25° - 75°E).

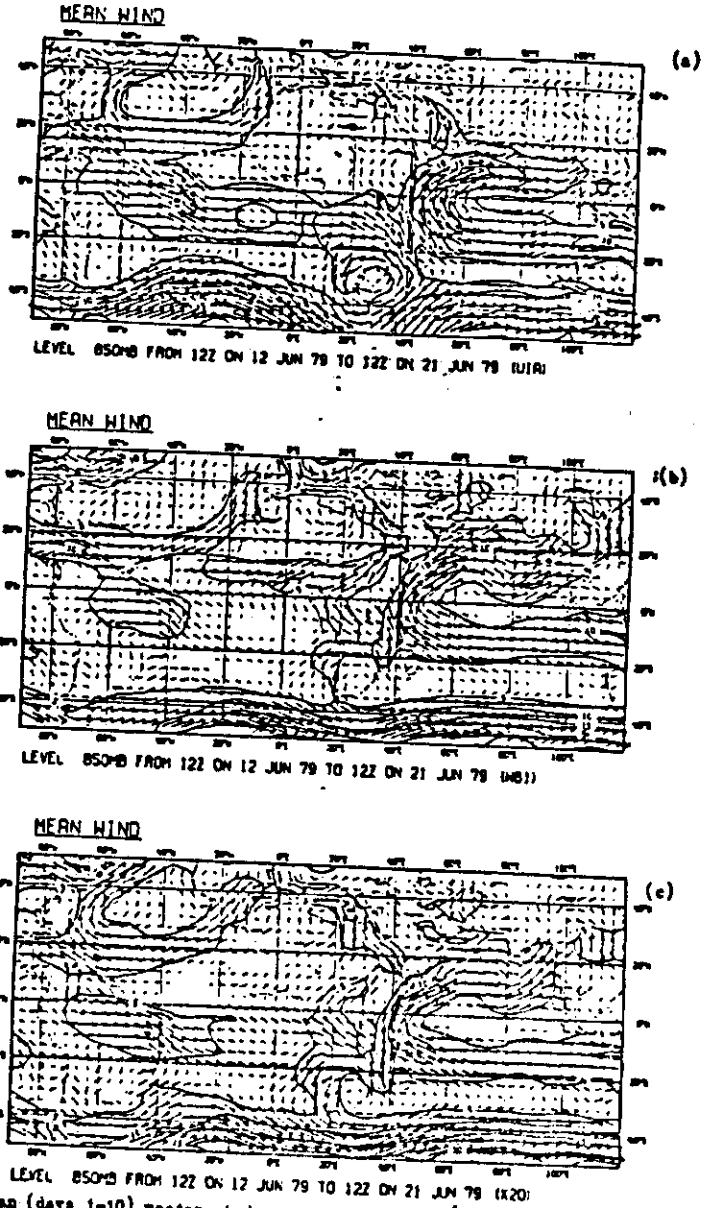

Fig. 7 Mean (days 1-10) vector winds and isotachs (ms^{-1}) at 850 mb (a) analysed field, (b) W81; (c) X20, (d) X31, (e) Y68; (f) BON.

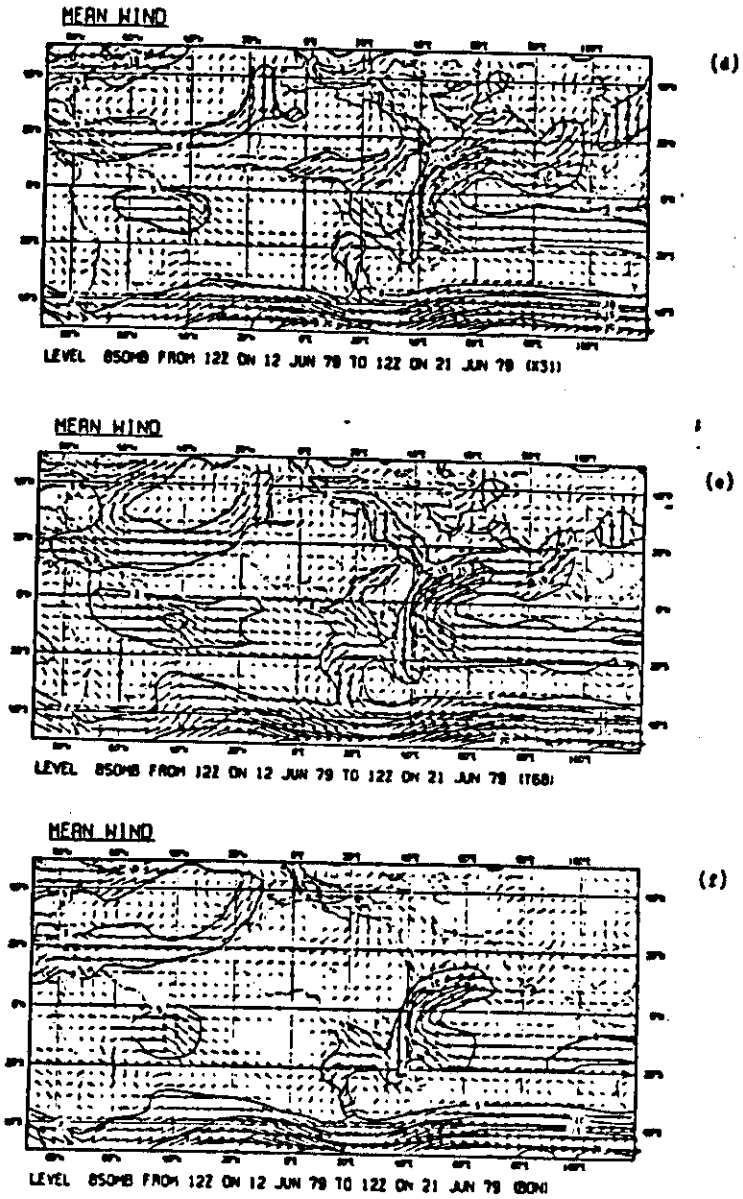

Fig. 7 (contd.)

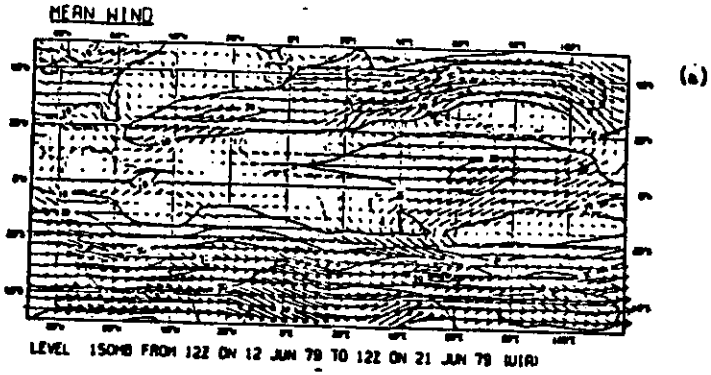

(a)

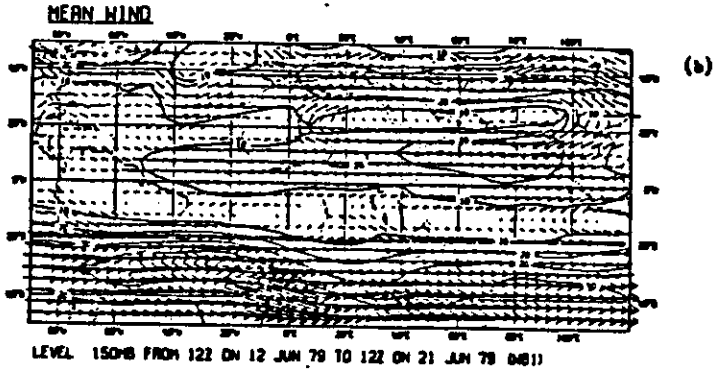

(b)

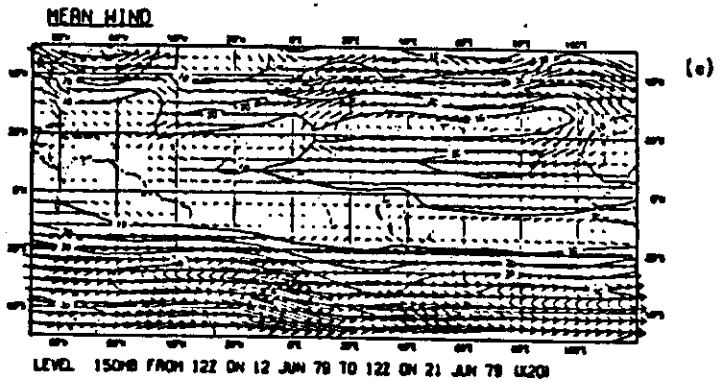

(c)

Fig. 8 Mean (days 1-10) vector winds and isotachs (ms^{-1}) at 150 mb. (a) analysed field; (b) W81, (c) X20; (d) X31; (e) Y68; (f) BON.

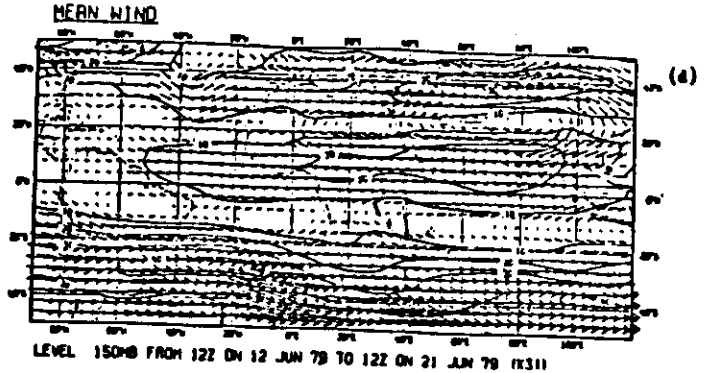

(d)

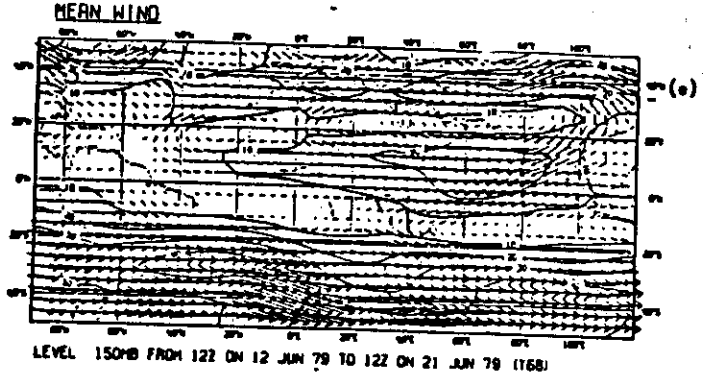

(e)

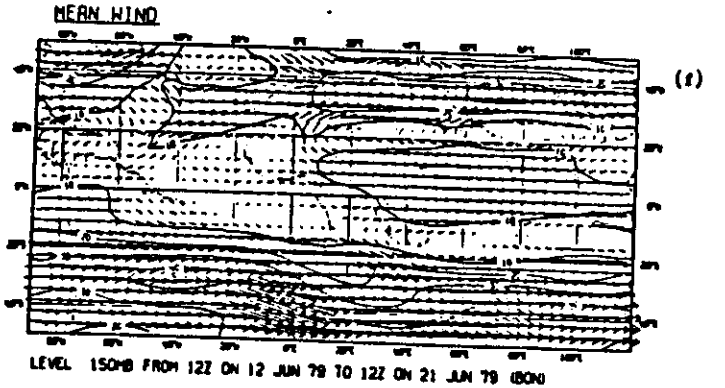

(f)

Fig. 8 (contd.)

F g. 9 Days 1-10 mean sectoral average (45° - 75°E) over the Arabian Sea of Zonal wind.
(a) analysed field; (b) W81; (c) X20; (d) X31; (e) Y68; (f) 80N.

Fig. 10 As fig. 9 for meridional wind

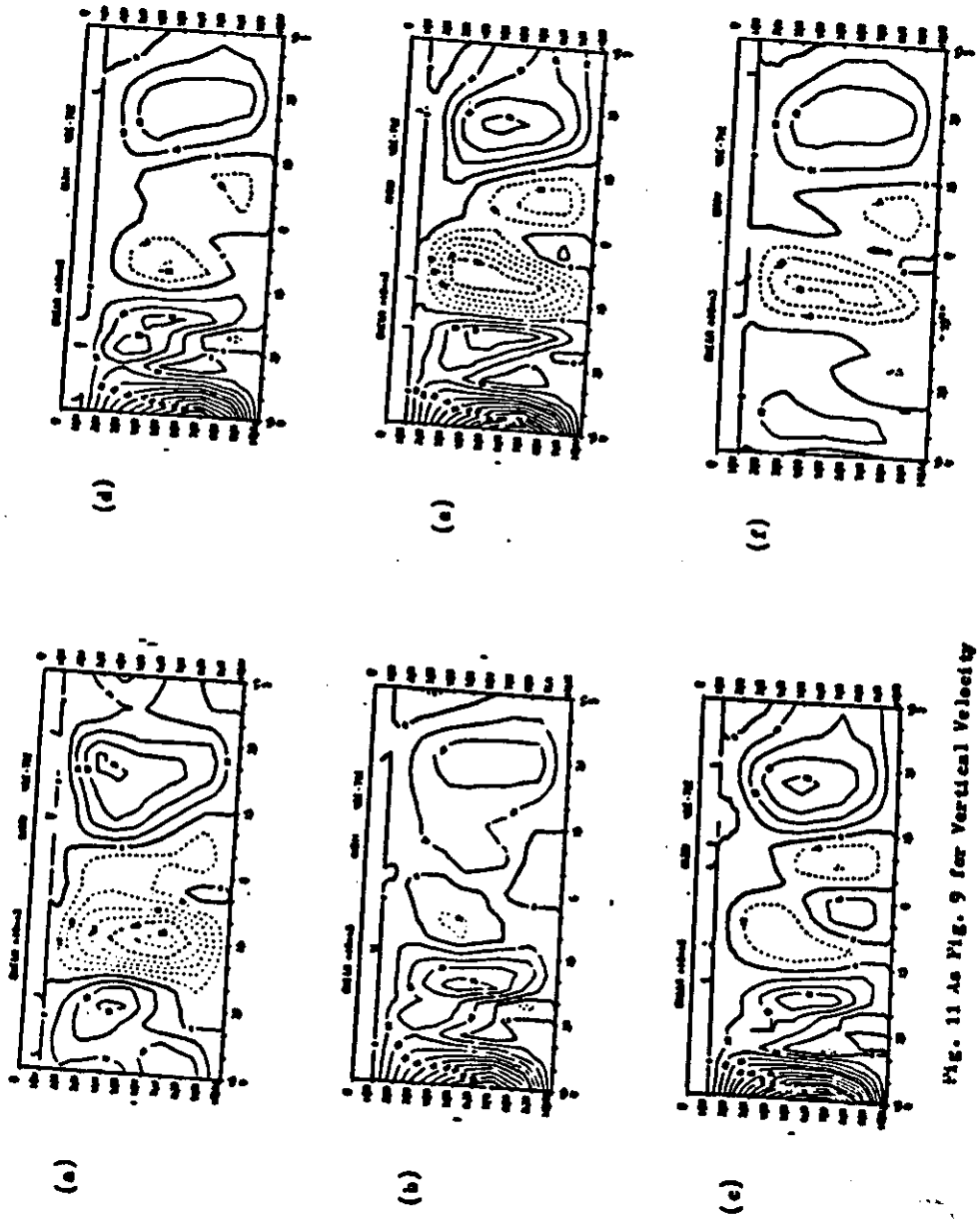

Fig. 11 As Fig. 9 for Vertical Velocity

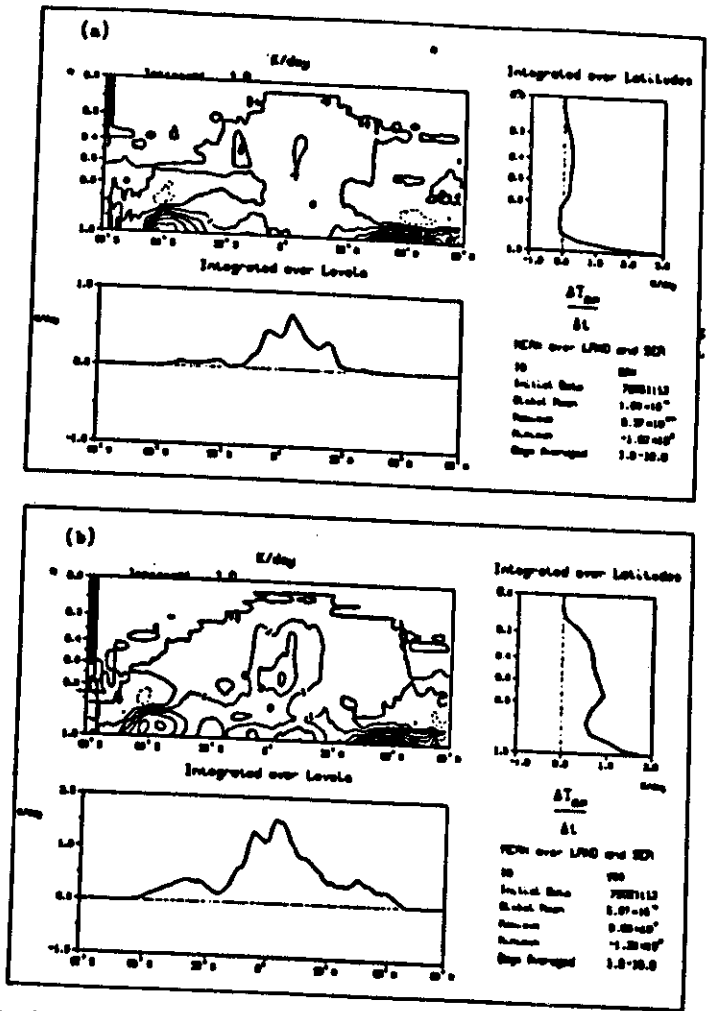

Fig. 12 : Days 1-10 mean temperature tendency due to cumulus convection in $K.day^{-1}$. (a) BOM; (b) Y68

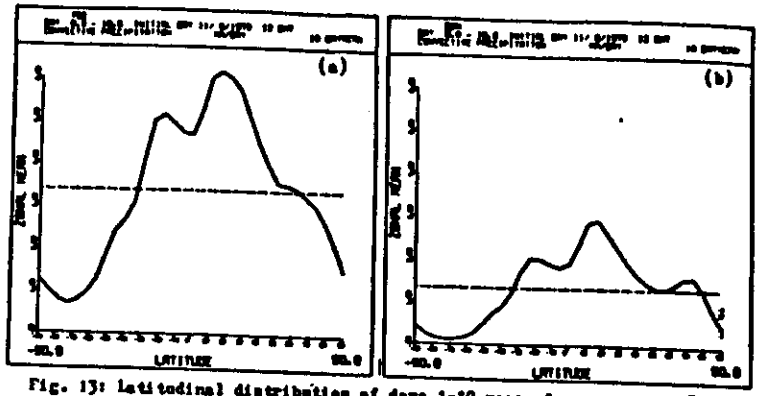

Fig. 13: Latitudinal distribution of days 1-10 mean of convective precipitation rate: (a) T63; (b) UCM

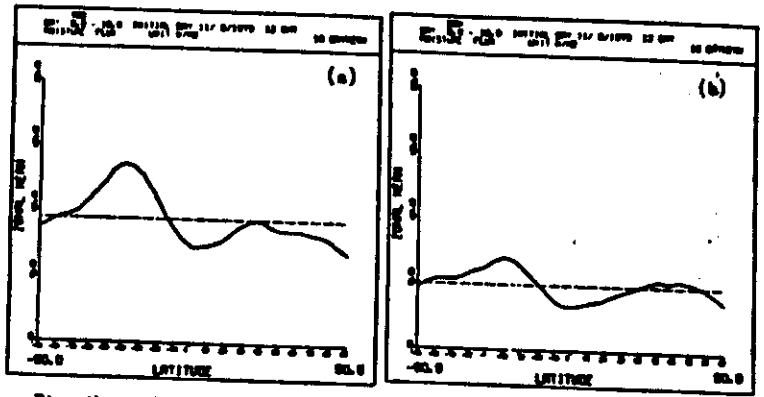

Fig. 14: As Fig.13 for surface moisture fluxes